**MERCURY SHAPE MODEL FROM LASER ALTIMETRY AND PLANETARY COMPARISONS.** Gregory A. Neumann[1], Mark. E. Perry[2], Erwan Mazarico[1], Carolyn M. Ernst[2], Maria T. Zuber[3], David E. Smith[3], Kris J. Becker[4], Robert E. Gaskell[5], James W. Head[6], Mark S. Robinson[7], and Sean C. Solomon[8,9], [1]NASA Goddard Space Flight Center, Greenbelt, MD 20771, USA (gregory.a.neumann@nasa.gov); [2]The Johns Hopkins University Applied Physics Laboratory, Laurel, MD 20723, USA; [3]Department of Earth, Atmospheric and Planetary Sciences, Massachusetts Institute of Technology, Cambridge, MA 02129-4307, USA; [4]Astrogeology Science Center, United States Geological Survey, Flagstaff, AZ 86001; [5]Planetary Science Institute, 1700 East Fort Lowell, Suite 106, Tucson, AZ 85719, USA; [6]Department of Earth, Environmental and Planetary Sciences, Brown University, Providence, RI 02886; [7]School of Earth and Space Exploration, Arizona State University, Tempe, AZ 85287, USA; [8]Lamont-Doherty Earth Observatory, Columbia University, Palisades, NY 10964, USA. [9]Department of Terrestrial Magnetism, Carnegie Institution of Washington, Washington, DC 20015, USA.

**Introduction:** The accurate determination of shape is essential for understanding the geology and geophysics of Mercury [1]. The Mercury Laser Altimeter (MLA) [2] has determined precisely [3] the topography of the northern hemisphere, complemented in the southern hemisphere by radio science (RS) occultation measurements [4]. Global digital elevation models (DEMs) of Mercury derived from flyby and orbital images via limb profiling [5], stereophotogrammetry [6, 7], and stereophotoclinometry [8] and the shape parameters obtained from spherical harmonic analysis can be compared with the shape determined by MLA.

**Data and methods:** MLA Reduced and Derived Data Records are submitted for MESSENGER release 15 in early May 2016. The dataset includes Mercury flybys 1 and 2 and Mercury orbital data ending on 30 April 2015. The altimetry comprises 40,690,416 altimetric observations of more than 26 million individual footprints (some on multiple channels), with meter-level precision and ~10-m radial accuracy, sampling 87% of the 0.5° by 0.5° pixels north of the equator and more sparsely to 16°S. To the 378 previously published [4] occultation measurements of radius at tangent points are added 179 measurements since the last release. To remove the bias relative to MLA resulting from topographic extremes, occultation locations and average radii have been adjusted with a local DEM [8].

We compare the resulting global dataset to a DEM derived from a bundle-adjusted control point network of Mercury Dual Imaging System (MDIS) narrow-angle camera (NAC) and multispectral wide-angle camera (WAC) images [9, 10].

The body-fixed registration of altimetric measurements from spacecraft uses a model of planetary orientation, originally intended to coincide with the principal axes of the body, as given by the text kernel pck00010_msgr_v21.tpc derived from MESSENGER-era data. The current model revises the rotation pole and rate and the prime meridian so as to place a previously adopted landmark at a -20°E longitude, shifting the registration of altimetric maps by as much as 0.1°, or 3–4 km at the equator, the differences arising from residual error in the old (pre-MESSENGER) control solution. Spherical harmonic (SH) analysis is performed by damped, weighted least squares or by numerical quadrature after resampling and interpolation.

**Results:** An empirical power law [11] constrains the topographic spectral variance (Fig. 1) out to SH degree ~40, or 200 km feature size, below which the relief of unrelaxed craters and/or noise increases the relative variance. The ~120-m center-of-figure offset given by the degree 1 terms is much less than that of Earth, the Moon, or Mars.

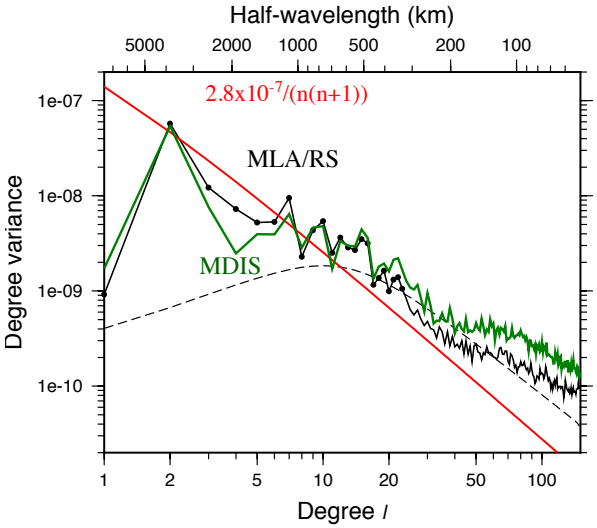


Figure 1. Comparison of degree variances (dimensionless) scaled to a mean radius of 2439.4 km. MLA/RS solution (dots) is shown with its formal uncertainty (dashed curve) and the empirical power law (red) used to regularize the least squares solution. SH coefficients are normalized [4].

The mean radius for the MDIS solution is 75 m larger than for the MLA/RS solution, and the oblateness and elongation are ~5% smaller (Table 1). The most noticeable differences are the reduced degree 4 variance (Fig. 1) and the cross-shaped residual as seen from the north pole (Fig. 2). The MDIS-derived shape is substantially more spherical at degree 4, its (4,4)

sectoral shape having only 1/6 of the MLA/RS solution amplitude (220 m) at the equator.

**Discussion:** Low-degree biases in image-based DEMs could arise from the Mercury thermal environment and resultant changes in camera focal length or could be related to sampling density. These biases should be mitigated by future work. The altimeter is affected somewhat by the oblique pointing required to protect the spacecraft during dayside operations, but the accuracy of the laser footprint elevation is mainly set by the precision in the spacecraft orbits and timing system [3] and is insensitive to temperature variations. The global shape model (pds-geosciences.wustl.edu/messenger/mess-h-rss_mla-5-sdp-v1/messrs_1001/data/shadr/gtmes_150v05_sha) is accurate in the northern hemisphere, but not sufficiently constrained in the southern hemisphere by the MLA/RS data because of undersampling. Future laser altimetric measurements by the BepiColombo mission, particularly in the southern hemisphere, may help resolve long-wavelength discrepancies in the shape of Mercury.

**References:** [1] Zuber M. T. et al. (2007) *Space Sci. Rev.,* 131, 105–132. [2] Cavanaugh J. F. et al. (2007) *Space Sci. Rev.,* 131, 451–479. [3] Zuber M. T. et al. (2012) *Science,* 336, 217–220. [4] Perry M. E. et al. (2015) *Geophys. Res. Lett.*, 42, 6951–6958. [5] Oberst J. et al. (2011) *Planet. Space Sci.* 59, 1916–1924. [6] Preusker F. et al. (2011) *Planet. Space Sci.* 59, 1910-1917. [7] Becker K. J. et al. (2014) *LPS*, 44, abstract 2829. [8] Gaskell, R. W. et al. (2008) *Meteorit. Planet. Sci.*, 43, 1049–1061. [9] Hawkins S. E. III. et al. (2007) *Space Sci. Rev.*, 131, 247–338. [10] Becker K. J. et al. (2016), *LPS*, 47, this meeting. [11] Bills B. G. and Kobrick M. (1985) *J. Geophys. Res.* 90, 827–836.

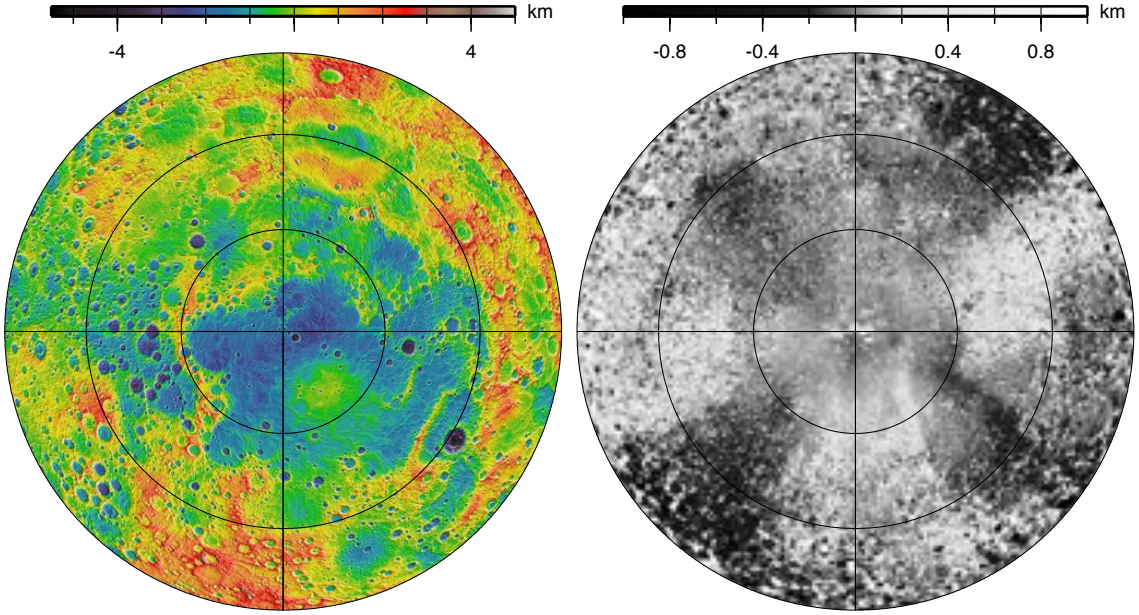


Figure 2. (a) Topography of the northern hemisphere of Mercury over shaded relief from MLA in Lambert equal-area projection, with 0° longitude at the bottom. (b) Difference between MDIS control point solution and MLA altimetry after binning at 1/16 by 1/16 degree per pixel, in the same projection as (a).

| SH Coefficient | MDIS, normalized | MLA/RS normalized | MLA/RS unnormalized | Comments |
|---|---|---|---|---|
| $C_{0,0}$ | 2439.470 | 2439.402±0.03 | 2439.402±0.03 | Mean radius |
| $C_{1,0}$ | -0.076 | -0.058±0.032 | -0.100±0.055 | COF-Z |
| $C_{1,1}$ | 0.028 | -0.008±0.026 | -0.014±0.045 | COF-X |
| $S_{1,1}$ | 0.061 | 0.045±0.031 | 0.079±0.054 | COF-Y |
| $C_{2,0}$ | -0.466 | -0.487±0.025 | -1.089±0.056 | Polar flattening |
| $\|\|C_{22}, S_{22}\|\|$ at -15.7°E | 0.314 | 0.323±0.038 | 0.214±0.025 | Equatorial ellipticity |

Table 1. Low-degree coefficients of the MDIS and MLA/RS shape models in km with 1-s.d. formal uncertainties.